JGR Oceans

RESEARCH ARTICLE
10.1029/2022JC019335

Sources and Sinks of Interannual Steric Sea Level Variability

Antoine Hochet[1], William Llovel[1], Florian Sévellec[1], and Thierry Huck[1]

[1]Laboratoire d'Océanographie Physique et Spatiale, CNRS, University of Brest, IFREMER, IRD, Plouzané, France

Key Points:

- The main source of interannual steric sea level variance is the advection of the mean density by interannual velocity anomalies
- This source of variance is balanced by fluctuating net heat flux from the atmosphere and by the fluctuating eddy induced velocities
- The main source of interannual steric sea level variance is mostly sustained by the wind variability via Ekman velocities

Correspondence to:
A. Hochet,
ahochet@ifremer.fr

Citation:
Hochet, A., Llovel, W., Sévellec, F., & Huck, T. (2023). Sources and sinks of interannual steric sea level variability. *Journal of Geophysical Research: Oceans*, *128*, e2022JC019335. https://doi.org/10.1029/2022JC019335

Received 27 SEP 2022
Accepted 29 MAR 2023

Abstract Understanding the mechanisms of regional steric sea level variability is fundamental to understand the regional sea level variability recorded by satellite altimetry for years and to insure that future projections made by climate models are realistic. Here, we first develop a novel method based on steric sea level variance budget that allows to detect the sources and sinks of the variability. Using the "Estimating the Circulation and Climate of the Ocean" (ECCO V4) state estimate, we then show that interannual steric sea level variability is mainly sustained by interannual fluctuating winds via Ekman transport almost everywhere. The damping of the variability is made by both the interannual fluctuating net heat flux from the atmosphere, that largely dominates the atmospheric freshwater fluxes, and the parametrized effect of eddies. It is also found that the parametrized effect of diffusion on the variability is weak in most regions and that, although globally weak, the fluctuations of atmospheric freshwater fluxes are a source of variance close to the Equator in the Pacific Ocean.

Plain Language Summary Since the launch of Topex/Poseidon satellite in August 1992, sea level is routinely measured every ~10 days at a nearly global coverage. For the first time, satellite altimetry data show that regional sea level trends experience large regional variability compared to its global mean trend. If global mean sea level rise is a direct consequence of the on-going climate change, regional sea level change is more relevant for coastal impacts. Thus, investigating the regional sea level changes and its causes are of great importance for potential socio-economic impacts as 10% of the world's population live at less than 10 m above sea level. Those investigations are also important for assessing the reliability of coupled climate models used to predict future sea level changes. In this study, we develop a novel method based on the steric sea level variance budget to rigorously estimate the sources and sinks of the interannual steric sea level variability so as to understand the physical processes at play. We find the main source of interannual steric sea level variance is the advection of the mean density by interannual velocity anomalies which are sustained by the wind variability via Ekman velocities.

1. Introduction

Sea level change is one of the most direct consequences of the on-going climate change and may have several socio-economical coastal implications (Nicholls & Cazenave, 2010). Sea level change has been routinely recorded, with a nearly global coverage, by satellite altimetry missions since the launch of Topex/Poseidon in 1992 and its successors (Jason-1/2/3, ENVISAT, ERS1/2, Saral/Altika, Cryosat-2, and more recently Sentinel6-MF, etc). These high-quality data have demonstrated that the global mean sea level experiences a linear rise of 3.3 mm yr^{-1} over the 1993–2015 period (WCRP Global Sea Level Budget Group, 2018). The global mean sea level is a good indicator of global warming but regional changes are most relevant for socio-economic impacts as roughly 10% of the world's population lived at less than 10 m above sea level especially in low-lying coastal and deltaic regions (Durand et al., 2019; Neumann et al., 2015). For the first time, satellite altimetry data have revealed that sea level is not rising uniformly and presents large deviations from its global mean trend. Indeed, some regions experience a linear rise 3 times as large as the global mean sea level trend [for instance in the western Pacific ocean, in the Indian ocean, and in the south Atlantic ocean for the 2005–2013 period; Cazenave and Llovel (2010); Llovel and Lee (2015)].

Superimposed to the long-term trends, regional sea level interannual variability can enhance or reduce regional sea level change. This interannual variability of sea level is driven by modes of climate variability such as El Nino Southern Oscillation, the North Atlantic Oscillation, and the Indian Ocean Dipole in the north Indian Ocean (Llovel et al., 2010). This interannual variability has a steric origin: it is due to variations of temperature and salinity affecting density, resulting from changes in surface wind stress and buoyancy fluxes (Stammer et al., 2013). Therefore, investigating the interannual variability of steric sea level and their mechanisms appears

to be highly relevant for understanding processes at play in regional sea level interannual variability. Moreover, understanding the interannual variability of regional sea level is essential to interpret satellite-based sea level observations relevant to ocean climate and to assess the reliability of future sea level projections made by coupled climate models.

Physical processes contributing to interannual variability of regional steric sea level have been studied using an observationally-constrained ocean state estimate produced by the "Estimating the Circulation and Climate of the Ocean" (ECCO) consortium (Meyssignac et al., 2017; Piecuch & Ponte, 2011). Piecuch and Ponte (2011) investigated the tendency changes of the vertically-integrated sea water density (i.e., steric sea level) due to fluctuating potential temperature and salinity. The tendencies of both tracers (potential temperature and salinity) are investigated by considering the conservation equation representing the effects of ocean advection, diffusion, and surface exchanges. This study suggested that the oceanic transports are more important than the surface buoyancy fluxes in setting the interannual variations of the steric sea level and that diffusion plays an important role at extratropical latitudes. This method has been widely used for identifying the physical processes at play in steric sea level interannual variability. However, this method presents some limitations as we cannot assess if the physical processes at play create or reduce the interannual steric sea level variability, in other words, if the physical process is a source or a sink of the interannual steric sea level variability.

Here we develop a novel method, based on the budget of the interannual steric sea level variance, to rigorously compute its sources and sinks and better understand its mechanisms. For this purpose, we use the ECCO V4 state estimate (Forget et al., 2015). The steric sea level variance budget is inspired from budget of density variance that were originally used to study the drivers of a multidecadal mode of variability in idealized simulations of the North Atlantic (Arzel et al., 2006; Colin de Verdière & Huck, 1999), in realistic configuration of the North Atlantic (Arzel et al., 2018; Gastineau et al., 2018), and mooring observations (Sévellec et al., 2021). Temperature variance budget have also been used in Hochet et al. (2020) to show that the non-linear transfer of temperature variance is directed from low to high frequencies. Here we transpose and adapt this approach to diagnose and partition as sources and sinks physical processes (advection, diffusion, and surface forcing) at play in the interannual steric sea level variability.

The remainder of this article is organized as follows: in Section 2 we describe the method to obtain the steric sea level interannual variance budget. In Section 3, we present the ECCO V4r3 state estimate. In Section 4, the different terms of the steric sea level variance budget in the ECCO V4r3 state estimate are obtained. In Section 5 we show how the steric sea level budget is related to the more classical density variance budget already used in numerous previous studies. In Section 6, we summarize and discuss the main conclusions of our study.

2. Method: Steric Sea Level Variance Budget

Based on the hydrostatic and Boussinesq approximations, the barometrically-corrected sea level can be partitioned into local density change (due to change in temperature and salinity; this term is known as steric sea level) and local/regional mass change [known as manometric sea level, see Gregory et al. (2019) for more details on these terminologies].

$$\eta = \eta_{\text{steric}} + \eta_{\text{manometric}} = -\frac{1}{\rho_s}\int_{-H}^{0} \rho \, \mathrm{d}z + \frac{P_b}{\rho_0 g}, \tag{1}$$

where g is the acceleration due to gravity, H is the total ocean depth, ρ_s is a time and spatially constant representative surface density, ρ is the in situ density, and P_b is the ocean bottom pressure (Gill & Niiler, 1973). We use $\rho_s = \rho_0 = 1{,}029$ kg m^{-3} in the remainder of this paper. Although manometric sea level variations are locally important at high latitudes, steric sea level variations are the main cause of interannual sea level variability in most regions (Carret et al., 2021; Lombard et al., 2005; Piecuch & Ponte, 2011) and is therefore the focus of this work. In what follows, we thus only consider the variations of η_{steric}.

The first step in computing the interannual steric sea level variance budget is to decompose every variable X into a time mean, an interannual component, and a high-frequency component:

$$X = \overline{X} + X^{\text{inter}} + X^{\text{HF}}, \tag{2}$$

where X is any time-dependent variable, $\overline{X}$ represents the time mean of X over the considered period of time, X^{inter} the interannual component of X which contains all frequencies strictly lower than the seasonal cycle, and X^{HF} the remaining high-frequency component of X which contains all the resolved frequency higher than annual

including the seasonal cycle. The time derivative of the steric sea level equation gives the local evolution equation of its variations:

$$\frac{\partial \eta^{\text{inter}}_{\text{steric}}}{\partial t} = -\frac{1}{\rho_0}\int_{-H}^{0} \frac{\partial \rho^{\text{inter}}}{\partial t}\,\mathrm{d}z, \tag{3}$$

where t is time. As mentioned in the introduction, the main novelty of this work is to compute the local variance budget of the steric sea level. Because we are interested in the mean sources and sinks over the considered period of time, the budget is obtained as the time average of the product of the interannual steric sea level equation and its evolution from Equation 3:

$$\overline{\eta^{\text{inter}}_{\text{steric}} \frac{\partial \eta^{\text{inter}}_{\text{steric}}}{\partial t}} = \overline{\frac{1}{2}\frac{\partial \left(\eta^{\text{inter}}_{\text{steric}}\right)^2}{\partial t}} = \overline{\frac{1}{\rho_0^2}\int_{-H}^{0} \rho^{\text{inter}}\,\mathrm{d}z \int_{-H}^{0} \frac{\partial \rho^{\text{inter}}}{\partial t}\,\mathrm{d}z}. \tag{4}$$

This demonstrates that this product is equal to the variations of the interannual steric sea level variance. To decompose the different terms of this budget, we thus need an evolution equation for ρ^{inter}. As in ECCO (Forget et al., 2015), we use the Jackett and Mcdougall (1995) equation of state for density to link the density to the potential temperature θ and the salinity S and pressure:

$$\rho = \rho(S, \theta, -\rho_0 g z), \tag{5}$$

where the pressure is assumed to be a function of only depth (z). Then, the time derivative of Equation 5 gives the evolution equation for ρ as a function of θ and S:

$$\begin{aligned}\frac{\partial \rho}{\partial t} &= \rho_0\left(-\alpha\frac{\partial \theta}{\partial t} + \beta\frac{\partial S}{\partial t}\right)\\ &= \underbrace{-\rho_0\alpha \mathrm{ADV}_\theta + \rho_0\beta \mathrm{ADV}_S}_{=\mathrm{ADV}} \underbrace{-\rho_0\alpha \mathrm{DIF}_\theta + \rho_0\beta \mathrm{DIF}_S}_{=\mathrm{DIF}} \underbrace{-\rho_0\alpha \mathrm{FLU}_\theta + \rho_0\beta \mathrm{FLU}_S}_{=\mathrm{FLU}}\end{aligned} \tag{6}$$

where $\mathrm{ADV}_{\theta,S}$, $\mathrm{DIF}_{\theta,S}$, and $\mathrm{FLU}_{\theta,S}$ represent respectively the θ, S advection, the parameterized diffusion of temperature and salinity, and the net heat flux and freshwater fluxes from the atmosphere. ECCO V4r3 provides all the necessary terms to close the temperature and salinity budgets. Temperature and salinity advection and diffusion are obtained from the divergence of the corresponding advective flux and diffusive flux which are direct outputs of the state estimate. Similarly, FLU_θ and FLU_S are also obtained from the direct outputs of ECCO V4r3. $\alpha = -1/\rho_0 \partial\rho/\partial\theta$ and $\beta = 1/\rho_0 \partial\rho/\partial S$ are respectively the thermal expansion and saline contraction coefficients obtained from the Jackett and Mcdougall (1995) equation of state for density. Note that the advection term regroups the resolved and parameterized eddy-induced transport; whereas the diffusion term regroups the isopycnal, diapycnal and convective mixing collectively. Using Equation (6), the equation for the interannual variations of density is thus:

$$\frac{\partial \rho^{\text{inter}}}{\partial t} = \mathrm{ADV}^{\text{inter}} + \mathrm{DIF}^{\text{inter}} + \mathrm{FLU}^{\text{inter}}, \tag{7}$$

where $\mathrm{ADV}^{\text{inter}}$ represents, the effect of advective terms, $\mathrm{DIF}^{\text{inter}}$ the effect of diffusive terms, and $\mathrm{FLU}^{\text{inter}}$ the buoyancy forcing from the atmosphere. Then, inserting Equation 7 in Equation 4 allows us to separate the steric sea level variance budget into advective, diffusive, and atmospheric fluxes contributions:

$$\overline{\frac{1}{2}\frac{\partial \left(\eta^{\text{inter}}_{\text{steric}}\right)^2}{\partial t}} = \overline{\mathrm{ADV}_{\text{steric}}} + \overline{\mathrm{DIF}_{\text{steric}}} + \overline{\mathrm{FLU}_{\text{steric}}} \tag{8}$$

where:

$$\overline{Y_{\text{steric}}} = \frac{1}{\rho_0^2}\overline{\int_{-H}^{0} \rho^{\text{inter}}\,\mathrm{d}z \int_{-H}^{0} Y\,\mathrm{d}z} \tag{9}$$

Y represents either $\mathrm{ADV}^{\text{inter}}$, $\mathrm{DIF}^{\text{inter}}$ or $\mathrm{FLU}^{\text{inter}}$. The main advantage of this method (variance budget) compared to the direct budget of η_{steric} is that it gives the local sources and sinks of the variability: if $\overline{Y_{\text{steric}}}$ is positive

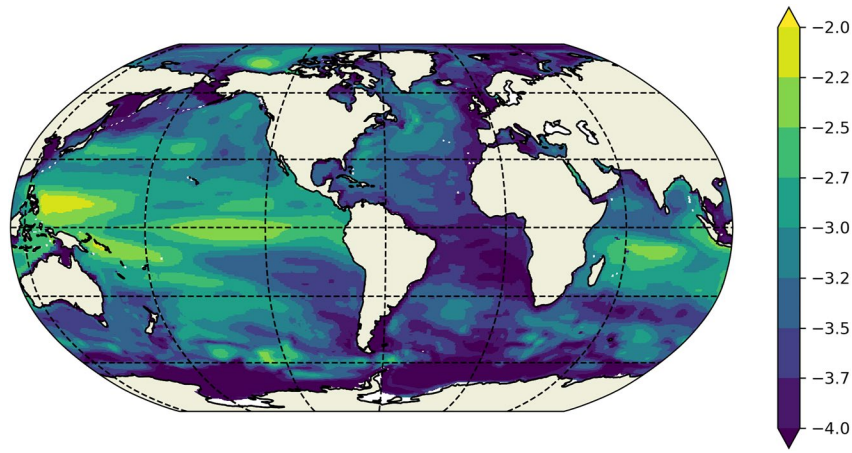

Figure 1. Time-variance of the interannual steric sea level (log scale, in m^2) obtained from the ECCO V4r3 state estimate and averaged over the period 1993–2014.

(negative) then it is a source (sink) of steric sea level variance because it acts to increase (decrease) $\eta^{\text{inter}}_{\text{steric}}$ variance. Equation 9 can also be written as:

$$\overline{Y_{\text{steric}}} = \overline{\eta^{\text{inter}}_{\text{steric}} B} \tag{10}$$

where $B = \frac{-1}{\rho_0} \int_{-H}^{0} Y \, dz$. It is then apparent that $\overline{Y_{\text{steric}}}$ can be a source in two different cases: (a) $\eta^{\text{inter}}_{\text{steric}}$ is positive and B is positive or (b) $\eta^{\text{inter}}_{\text{steric}}$ is negative and B is negative. It is also interesting to note that it is the correlation between the vertical integral of the density anomaly and the vertical integral of the interannual anomaly of advection, diffusion, or buoyancy surface flux that creates a sink or a source of steric sea level variance. Therefore, in Equation 9 ρ^{inter} and Y do not need to be correlated at the same depths to create a source or a sink.

The results of the steric sea level variance budget applied to ECCO V4r3 outputs, as given by Equation 8 will first be shown in Section 4.1. Then the advective term of the budget $\left(\overline{\text{ADV}_{\text{steric}}}\right)$ will be further decomposed into four different terms in Section 4.2.

3. Model

We assess the steric sea level variance budget using the ECCO V4r3 state estimate that covers the 1992–2017 period. This reanalysis is the output of the Massachusetts Institute of Technology general circulation model (MITgcm) assimilating available observations for the period 1992 to 2017 (Forget et al., 2015). The advantage of this reanalysis is that it satisfies the equation of motion and conservation laws hence making it possible to compute tracers budget. The solution used in this article is computed on the LLC90 grid which has an average horizontal resolution of 1° and 50 vertical levels. Outputs of the model consist of one month average and the closed budget can be obtained for the 1993–2014 period. Thus we compute the steric sea level budget over this 1993-2014 period.

Interannual anomalies are computed by removing the time mean seasonal cycle from the monthly time series, then the subannual signal is removed using a Lanczos low-pass filter with a 1 year cutoff frequency. The interannual variability defined here thus contains all periods longer than 13 months (including the regional long-term steric sea level trends).

The interannual steric sea level variance computed from the ECCO V4r3 estimate (Figure 1) shows, in agreement with previous studies (Piecuch & Ponte, 2011, for instance), the largest values at low latitudes in the equatorial Pacific and in the Indian ocean. At high latitudes, it is interesting to note that large interannual variability of the steric sea level are found in the Beaufort gyre of the Arctic ocean. Fukumori et al. (2021)

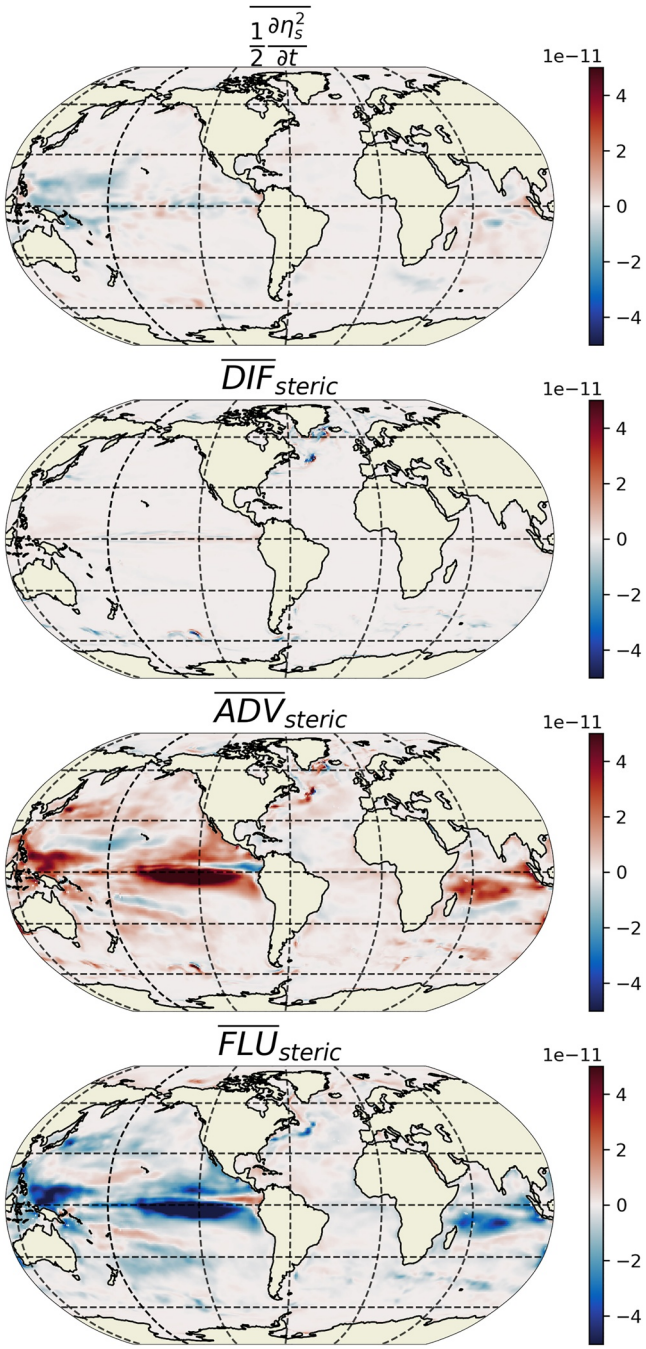

Figure 2. Terms of the interannual steric sea level variance budget (in $m^2\ s^{-1}$) for total (top), diffusion (second line), advection (third line), and atmospheric fluxes (last line). The spatial integral obtained for each terms is given in Table 1.

have shown that interannual variations in halosteric sea level in this region are linked with wind driven Ekman transport.

4. Interannual Steric Sea Level Variance Budget

In this section, we first present the decomposition of the interannual steric sea level variance budget as given by Equation 8, then derive the decomposition of the advective term and finally associate the advective source term with Ekman velocities.

4.1. Interannual Steric Sea Level Variance Budget

The interannual steric sea level variance budget indicates the relative importance of the different terms (Figure 2). $\overline{\mathrm{ADV}_{\mathrm{steric}}}$ is positive almost everywhere except in some localized regions of the western north Pacific low latitudes. The largest magnitudes are found in the eastern equatorial regions of the Pacific and Indian Ocean. On the contrary, $\overline{\mathrm{FLU}_{\mathrm{steric}}}$ is negative and compensates $\overline{\mathrm{ADV}_{\mathrm{steric}}}$ almost exactly. Table 1 gives the global integral of the different terms of the interannual steric sea level variance budget. As expected from the maps, the largest source is the advection $\left(\overline{\mathrm{ADV}_{\mathrm{steric}}}\right)$ with $4.8 \times 10^{-12}\ m^2\ s^{-1}$ and the largest sink is the atmospheric buoyancy flux $\left(\overline{\mathrm{FLU}_{\mathrm{steric}}}\right)$ with $-5 \times 10^{-12}\ m^2\ s^{-1}$. The damping of steric sea level variations by atmospheric buoyancy flux is mainly associated with the interannual variations of the net heat flux (see Figure 3 and Table 1) but variations of freshwater fluxes play a non-negligible role close to the equator in the Pacific ocean (acting as a source of variance). The net interannual atmospheric heat flux thus act to decrease the temperature when temperature anomalies are positive and to increase the temperature when temperature anomalies are negative. Overall, the main balance is therefore between the advection, which is a source of variance in almost all regions and the net atmospheric heat flux which is a sink of variance. This is one of the main results of this study which we believe has never been shown before. The amplitude of these two terms is almost one order of magnitude larger than the amplitude of the parameterized diffusive term $\left(\overline{\mathrm{DIF}_{\mathrm{steric}}}\right)$ and the time mean of the squared steric sea level anomaly tendency $\left(\overline{\frac{\partial \left(\eta_s^{\mathrm{inter}}\right)^2}{\partial t}}\right)$ (Figure 2). The strongest magnitude of the time mean squared steric sea level anomaly is found at low latitudes in the western Pacific and has negative values. These negative values are due to the decrease of the interannual variability over the ECCO V4r3 period (1993–2014). The term $\overline{\frac{\partial \left(\eta_s^{\mathrm{inter}}\right)^2}{\partial t}}$ would be zero in a stable climate (i.e., with a constant external forcing) and a time period sufficiently long to sample all the internal variability. Here, these two conditions are not satisfied: the climate is not stable because of anthropogenic climate change and the 22 years period (1993–2014) is too short to capture all the internal variability. The decrease of $\overline{\frac{\partial \left(\eta_s^{\mathrm{inter}}\right)^2}{\partial t}}$ in the western Pacific could therefore either be associated with anthropogenic climate change or with decadal natural variability, but this question is outside the scope of this article. The diffusion term $\left(\overline{\mathrm{DIF}_{\mathrm{steric}}}\right)$ is at least one order of magnitude smaller than the advective and atmospheric buoyancy flux terms and is weakly negative when integrated horizontally (Table 1).

Several authors (Llovel et al., 2010; Lombard et al., 2005) have shown that the interannual steric sea level variations in the Equatorial Pacific are associated with the El Niño-Southern Oscillation (ENSO). In the Indian Ocean,

Table 1
Globally-Averaged Terms Shown on Figures 2–4

Term	10^{-12} m^2 s^{-1}
Figures 2 and 3: $\left(\eta_s^{\text{inter}}\right)^2$ budget	
$\frac{1}{2}\frac{\partial\left(\eta_s^{\text{inter}}\right)^2}{\partial t}$	−0.4
$\overline{\text{DIF}_{\text{steric}}}$	−0.2
$\overline{\text{ADV}_{\text{steric}}}$	4.8
$\overline{\text{FLU}_{\text{steric}}}$	−5.0
$\overline{\text{FLU}_{\text{steric}}^{\text{THETA}}}$	−5.7
$\overline{\text{FLU}_{\text{steric}}^{\text{SALT}}}$	0.7
Figure 4: advection decomposition	
$\overline{\text{ADV}_{\text{steric}}^{1}}$	13.8
$\overline{\text{ADV}_{\text{steric}}^{2}}$	−1.4
$\overline{\text{ADV}_{\text{steric}}^{3}}$	1.1
$\overline{\text{ADV}_{\text{steric}}^{4}}$	−8.7

the interannual variations of the steric sea level have been shown to be associated with the Indian Ocean Dipole (IOD) (Llovel et al., 2010). Here we thus show that the main balance of the ENSO and IOD associated steric sea level variations is the forcing made by the advective term and the damping made by variations of net atmospheric heat flux.

4.2. Decomposition of the Advective Term

The advection term ADV can be expressed as a function of in-situ density by computing the product of the 3D velocity **v** and the gradient of the equation of state for density (5):

$$\text{ADV} = -\rho_0(-\alpha\nabla\cdot \text{v}\theta + \beta\nabla\cdot \text{v}S) = -\nabla\cdot \text{v}\rho_{\text{in situ}} - wg\gamma\rho_0 \qquad (11)$$

where $\gamma = 1/\rho_0\partial\rho/\partial p$ is the pressure expansion coefficient. Thus ADV represents the advection of in-situ density plus a term due to its pressure dependence. Assuming that γ is a constant, we can define a depth-dependent background density $\rho_B(z)$ that satisfies $\frac{\partial\rho_B}{\partial z} = \gamma g\rho_0$. Then, writing $\rho^* = \rho_{\text{in situ}} + \rho_B(z)$, we have:

$$\text{ADV} = -\nabla\cdot \text{v}\rho^* \qquad (12)$$

which shows that ADV can be interpreted as the advection of the in-situ density corrected from its pressure dependence that is, ρ^*. For the sake of

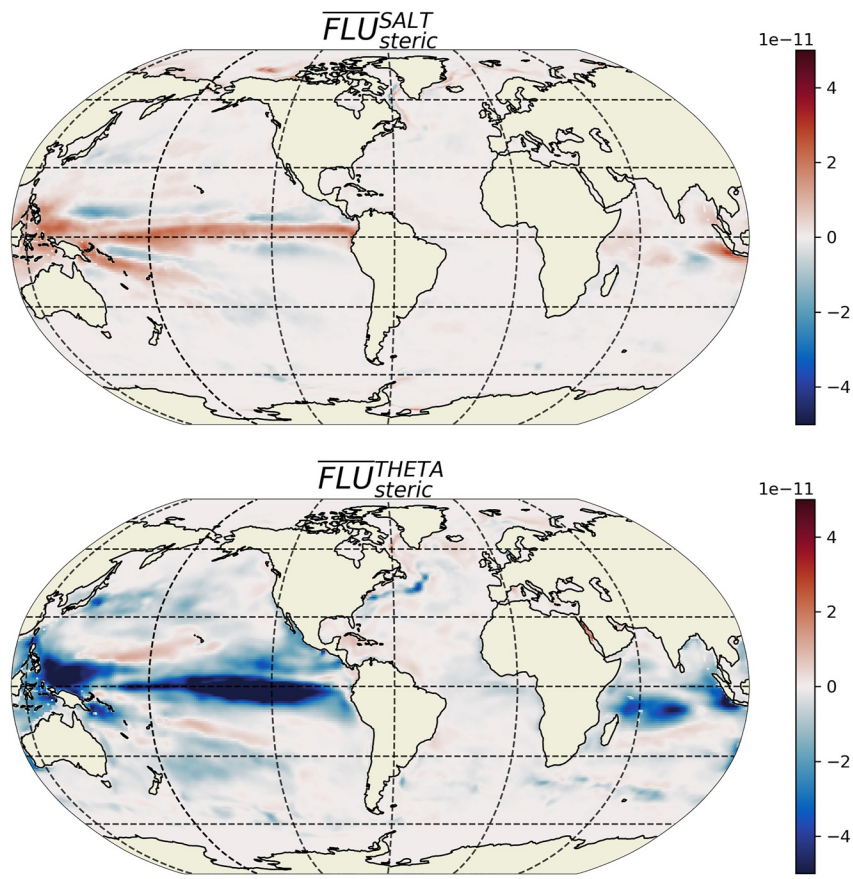

Figure 3. Decomposition of the atmospheric fluxes term ($\overline{\text{FLU}_{\text{steric}}}$, in m s^{-2}) into a part associated with salinity due freshwater fluxes (top panel) and a part associated with temperature and due to the net heat flux from the atmosphere (bottom panel). The spatial integral of the 2 terms is given in Table 1.

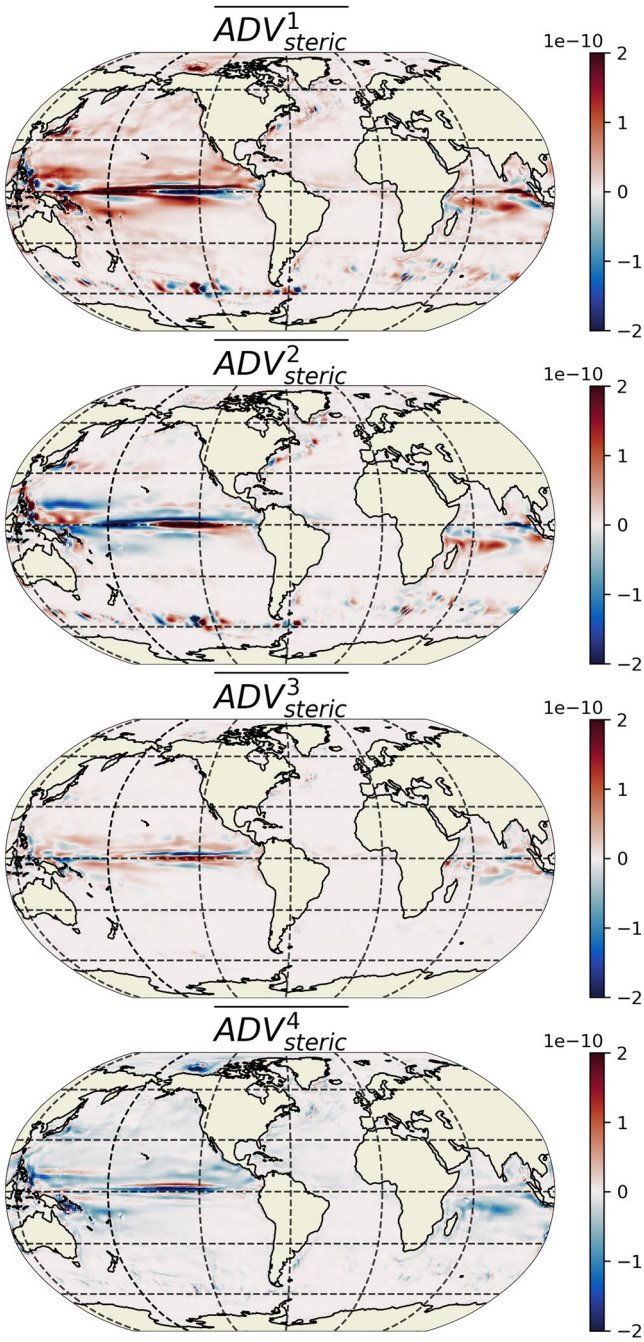

Figure 4. Decomposition of the advective term of the interannual steric sea level variability budget (in $m^2\ s^{-1}$) into: the advection of mean density by interannual velocity ($\overline{ADV^1_{steric}}$, top), the advection of interannual density by mean velocity ($\overline{ADV^2_{steric}}$, second row), the non-linear self advection of interannual density ($\overline{ADV^3_{steric}}$, third row), and the rectification effect of higher frequencies including the action of GM eddy-induced advection ($\overline{ADV^4_{steric}}$, bottom). The spatial integrals of the 4 terms are given in Table 1. The sum of these four terms gives the total advection shown in Figure 2, bottom left panel.

conciseness, we drop the * superscript in what follows. Note that in practise, all terms in the following density advection decomposition are computed from the decomposition of the temperature and salinity advection given by the first equality in Equation 11.

Using the timescale decomposition [Equation 2] from Section 2, the interannual advective term that appears in Equation 8 can be decomposed as:

$$\mathrm{ADV}^{\mathrm{inter}} = -\nabla\cdot(\mathbf{v}\rho)^{\mathrm{inter}} = \underbrace{-\nabla\cdot\mathbf{v}^{\mathrm{inter}}\overline{\rho}}_{=\mathrm{adv}_1} \underbrace{-\nabla\cdot\overline{\mathbf{v}}\rho^{\mathrm{inter}}}_{=\mathrm{adv}_2} \underbrace{-\nabla\cdot\mathbf{v}^{\mathrm{inter}}\rho^{\mathrm{inter}}}_{=\mathrm{adv}_3} + \underbrace{R^{HF}}_{=\mathrm{adv}_4}, \tag{13}$$

where adv_1 is the advection of mean density by interannual anomalous velocities, adv_2 is the advection of interannual density by mean velocities, adv_3 is the non-linear self advection of interannual density and adv_4 is the residual, containing the rectification effect of higher frequencies due to the correlation of submonthly velocity and submonthly density anomalies and the effect of Gent and McWilliams parameterized eddies (Gent & McWilliams, 1990, GM hereafter). (The expression for adv_4 is given in Appendix A for reference but is computed as a residual in practice.) Using Equation 13, the advective term of the steric sea level variance budget [see Equation 8] can thus be decomposed into four terms as:

$$\overline{\mathrm{ADV}_{\mathrm{steric}}} = \sum_{i=1}^{4} -\overline{\frac{\eta^{\mathrm{inter}}}{\rho_0}\int_{-H}^{0}\mathrm{adv}_i\,\mathrm{d}z} = \sum_{i=1}^{4}\overline{\mathrm{ADV}^i_{\mathrm{steric}}} \tag{14}$$

where the notation $\mathrm{ADV}^i_{\mathrm{steric}}$ is given by Equation (9) with $Y = \mathrm{adv}_i$. The four terms from the decomposition of the $\overline{\mathrm{ADV}_{\mathrm{steric}}}$ term are shown in Figure 4. In most of the regions, the advection of mean density by interannual velocity is positive although it can be negative in some localized regions (e.g., in the eastern Equatorial Pacific). Globally, it is the largest source of steric sea level variance (Figure 4 top left panel) with a horizontal average of $13.8\times10^{-12}\ m^2\ s^{-1}$. Locally this source term is balanced by both the advection of ρ^{inter} by mean velocities and by the HF rectification term. However, globally, the spatial integral of the two terms reveals that the main sink is the HF rectification term (horizontal average: $-8.7\times10^{-12}\ m^2\ s^{-1}$). Indeed, an important compensation occurs between the spatial integral of $\overline{\mathrm{ADV}^1_{\mathrm{steric}}}$ (source term) and the spatial integral of the rectification effect of higher frequencies (sink term). This HF rectification term is mostly the result of the GM parameterization of eddy induced velocities (not shown). Remarkably, the compensation between the source $\overline{\mathrm{ADV}^1_{\mathrm{steric}}}$ and the sink term due to the GM parameterization of eddies is locally important in the Beaufort gyre in the Arctic ocean where their sum almost cancel out. The term linked with the advection of interannual density anomalies by mean velocities, that is, $\overline{\mathrm{ADV}^2_{\mathrm{steric}}}$, is an important local sink of interannual steric sea level variance mainly in the western equatorial Pacific, it can also be a source in the equatorial eastern Pacific and western Indian ocean. When horizontally integrated $\overline{\mathrm{ADV}^2_{\mathrm{steric}}}$ is weakly negative. The term linked with the non-linear self advection of interannual density $\left(\overline{\mathrm{ADV}^3_{\mathrm{steric}}}\right)$ is, in most regions, negligible except at low latitudes where it is generally positive. Globally, the two main terms composing the advection part of the interannual steric sea level budget are thus: (a) a source term made by the advection of mean density by interannual velocities and (b) a sink term, mainly due to the GM parameterization of eddy velocities.

4.3. Role of Ekman Velocities in Interannual Steric Sea Level Variability

In this subsection, we show that $\overline{\mathrm{ADV}^1_{\mathrm{steric}}}$ can be explained by the direct effect of wind via Ekman velocities. To this end, we compute the term of the steric sea level variance budget that corresponds to the transport of mean density by interannual Ekman velocities:

$$\mathrm{ADV}^{\mathrm{Ekman}} = \frac{\eta^{\mathrm{inter}}}{\rho_0} \int_{-D_{\mathrm{ek}}}^{0} \nabla \cdot \mathbf{v}^{\mathrm{inter}}_{\mathrm{Ekman}} \overline{\rho} \mathrm{d}z \tag{15}$$

where $\mathbf{v}^{\mathrm{inter}}_{\mathrm{Ekman}}$ is the 3D interannual Ekman velocity in the Ekman layer whose depth D_{ek} is assumed everywhere constant. We assume that the horizontal Ekman velocities are 0 below the Ekman layer (i.e., $z < D_{\mathrm{ek}}$) and depth independent in the Ekman layer (for $0 > z > D_{\mathrm{ek}}$) and given by:

$$\left(u^{\mathrm{inter}}_{\mathrm{ek}}, v^{\mathrm{inter}}_{\mathrm{ek}}\right) = \frac{1}{D_{\mathrm{ek}} f_0 \rho_0} \left(\tau^{\mathrm{inter}}_y, -\tau^{\mathrm{inter}}_x\right) \tag{16}$$

where f_0 is the Coriolis parameter and $\left(\tau^{\mathrm{inter}}_x, \tau^{\mathrm{inter}}_y\right)$ are the zonal and meridional components of the interannual anomalies of momentum stress due to wind. Note that the momentum stress takes into account the effect of sea-ice at high latitudes. The vertical Ekman velocity in the Ekman layer is then obtained from the vertical integral of the continuity equation as:

$$w^{\mathrm{inter}}_{\mathrm{ek}}(z) = -z\left(\frac{\partial u^{\mathrm{inter}}_{\mathrm{ek}}}{\partial x} + \frac{\partial v^{\mathrm{inter}}_{\mathrm{ek}}}{\partial y}\right) \tag{17}$$

$\mathbf{v}^{\mathrm{inter}}_{\mathrm{Ekman}} = \left(u^{\mathrm{inter}}_{\mathrm{ek}}, v^{\mathrm{inter}}_{\mathrm{ek}}, w^{\mathrm{inter}}_{\mathrm{ek}}\right)$ in then used to compute $\mathrm{ADV}^{\mathrm{Ekman}}$ from Equation 15. We choose to use $D_{\mathrm{ek}} = 50$ m. Because the Ekman velocities are inversely proportional to D_{ek} and are vertically integrated over D_{ek}, we find that $\mathrm{ADV}^{\mathrm{Ekman}}$ is almost independent of the choice of D_{ek} (tested values: D_{ek} between 20 and 100 m) as already noticed by Buckley et al. (2014) for the variation of temperature in the mixed layer due to Ekman velocities. $\overline{\mathrm{ADV}^{\mathrm{Ekman}}}$ is shown in the top panel of Figure 5. Values are positive in most of the region and the largest magnitudes are found at low latitudes in qualitative agreement with $\overline{\mathrm{ADV}^1_{\mathrm{steric}}}$ (top panel, Figure 4). Positive values of $\overline{\mathrm{ADV}^{\mathrm{Ekman}}}$ are also found in the Beaufort gyre in the Arctic ocean, suggesting that the surface momentum stress is an important source of interannual steric sea level variance in this region. The fact that $\overline{\mathrm{ADV}^{\mathrm{Ekman}}}$ is qualitatively similar to $\overline{\mathrm{ADV}^1_{\mathrm{steric}}}$ suggests that $\overline{\mathrm{ADV}^1_{\mathrm{steric}}}$ is mainly contained to the surface Ekman layer. This is confirmed by the vertical integral in the Ekman layer of the term associated with adv_1 (top panel of Figure 5) that is,:

$$-\overline{\frac{\eta^{\mathrm{inter}}}{\rho_0} \int_{-D_{\mathrm{ek}}}^{0} \mathrm{adv}_1 \mathrm{d}z} \tag{18}$$

which is almost identical to $\overline{\mathrm{ADV}^1_{\mathrm{steric}}}$ (top panel, Figure 4). Note that we have also tested the reconstruction of $\overline{\mathrm{ADV}^2_{\mathrm{steric}}}$ using Ekman velocities, however, the agreement between the reconstruction and $\overline{\mathrm{ADV}^2_{\mathrm{steric}}}$ is low suggesting that other processes must be at play. This reconstruction is thus not shown.

In the Indian ocean, the main mode of interannual steric level variability is the Indian Ocean Dipole (Llovel et al., 2010), this dipole is associated with large scale SST variations forced by interannual wind variations (Saji et al., 1999). In agreement with this wind forced mode of variability, the interannual wind variations act as a source of steric sea level variability in the western part of the equatorial Indian basin. However, negative values are found in the Eastern part, which suggests that, in this region, interannual wind variations may also act as a sink of interannual steric sea level variability. Interestingly, the total effect of advection $\overline{\mathrm{ADV}_{\mathrm{steric}}}$ (see Figure 2) is always positive in the equatorial Indian region suggesting that the sink effect of wind variations is balanced by an advective source. Figure 4 reveals that both $\overline{\mathrm{ADV}^2_{\mathrm{steric}}}$ and $\overline{\mathrm{ADV}^3_{\mathrm{steric}}}$, respectively the advection made by the mean velocity and the self advection have positive values in this region and thus compensate the damping of interannual steric sea levels variability made by the wind.

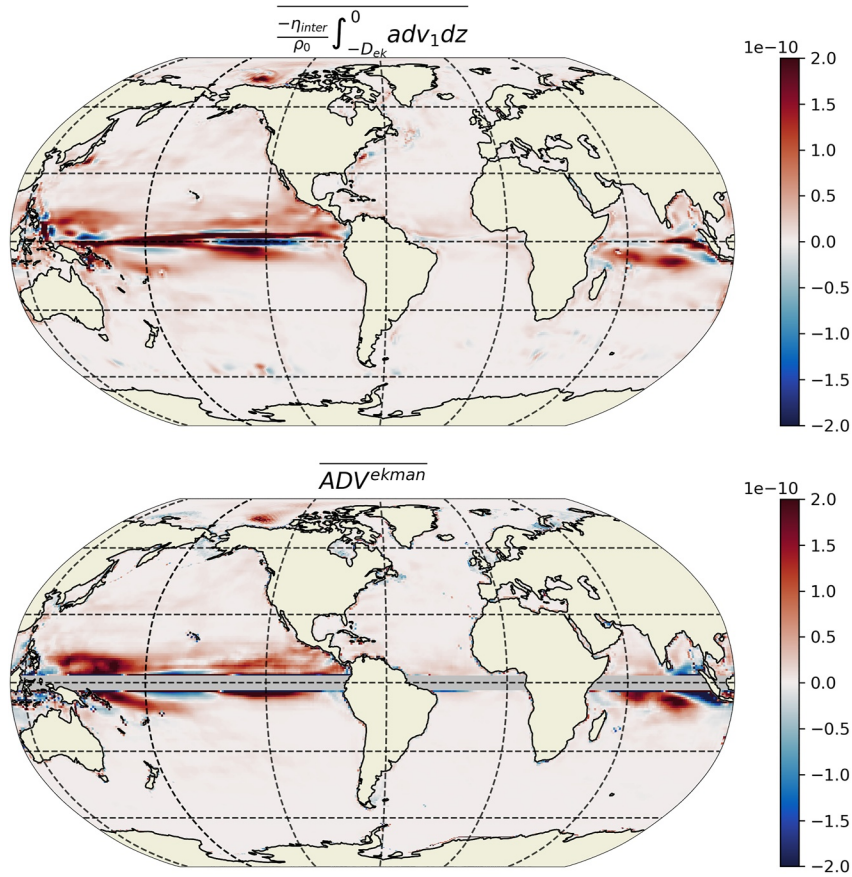

Figure 5. Top panel: same as $\overline{\mathrm{ADV}^{1}_{\mathrm{steric}}}$ (top panel, Figure 4) but where adv_1 is vertically integrated in the Ekman layer instead of over the full depth. Bottom panel: $\overline{\mathrm{ADV}^{\mathrm{Ekman}}}$ (in $\mathrm{m}^2\ \mathrm{s}^{-1}$): term associated with the advection of the mean density by 3D Ekman velocities, vertically integrated in the Ekman layer [see formula Equation 15]. The gray band close to the equator corresponds to the region where the Ekman balance does not hold.

5. Link Between Steric Sea Level Variance Budget and Density Variance Budget

In this section, we show that the steric sea level variance budget developed in the previous sections is proportional to the vertically integrated barotropic density variance budget. As will be explained below, the barotropic density variance budget is a component of the density variance budget which was used in many past studies (e.g., Arzel et al., 2018; Colin de Verdière & Huck, 1999; Gastineau et al., 2018; Huck et al., 1999) to understand the mechanisms of a multidecadal mode of variability in the North Atlantic. The use of the barotropic variance budget will allow us to interpret the different terms of the steric sea level variance budget as transfers of density variance between different density variance reservoirs. Additionally, density variance is close to the Quasi-Geostrophic (QG) Available Potential Energy (APE), indeed, interannual QG APE is associated to the interannual density variance through the following formula (see Vallis, 2017, for instance):

$$\mathrm{APE}^{\mathrm{inter}}_{\mathrm{QG}} = \frac{1}{2}\frac{g^2\left(\rho^{\mathrm{inter}}\right)^2}{\rho_0 N_s^2(z)}, \tag{19}$$

where $N_s^2(z)$ is the horizontally averaged Brunt Vaisala frequency. However, because $N_s^2(z)$ is depth dependent, $\mathrm{APE}^{\mathrm{inter}}_{\mathrm{QG}}$ is proportional to the vertically integrated density variance only where the $N_s^2(z)$ depth dependency is negligible.

5.1. Density Variance Decomposition

The interannual density anomaly can be decomposed into barotropic and baroclinic parts as:

$$\rho^{\text{inter}} = \rho^{\text{inter}}_{\text{BT}} + \rho^{\text{inter}}_{\text{BC}}, \tag{20}$$

where $\rho^{\text{inter}}_{\text{BT}}$ and $\rho^{\text{inter}}_{\text{BC}}$ are the barotropic and baroclinic parts of ρ^{inter}, respectively, with $\rho^{\text{inter}}_{\text{BT}}$ the vertically averaged density anomaly (i.e., $\rho^{\text{inter}}_{\text{BT}} = \frac{1}{H}\int_{-H}^{0} \rho^{\text{inter}} \mathrm{d}z$) and $\rho^{\text{inter}}_{\text{BC}} = \rho^{\text{inter}} - \rho^{\text{inter}}_{\text{BT}}$. Using the relationship between the density anomaly and the steric sea level given by Equation 1, we have:

$$\rho^{\text{inter}}_{\text{BT}} = -\frac{\rho_0}{H}\eta^{\text{inter}}. \tag{21}$$

Thus, steric sea level anomalies can also be interpreted as barotropic density anomalies. It should be noted that because it is well established that the interannual steric sea level variations are mainly due to density anomalies close to the ocean surface (Llovel et al., 2013; Willis et al., 2004), the barotropic interannual density anomalies therefore also mainly reflect surface density anomalies. Using Equation 2 to decompose the density ρ into different timescales and the vertical decomposition of the interannual density anomaly (Equation 20) gives:

$$\rho = \overline{\rho} + \rho^{\text{inter}}_{\text{BT}} + \rho^{\text{inter}}_{\text{BC}} + \rho^{\text{HF}}. \tag{22}$$

Using this decomposition, we show in Appendix B that the vertically integrated density variance is the sum of four terms:

$$\int_{-H}^{0} \overline{\rho^2}\,\mathrm{d}z = \int_{-H}^{0} \overline{\rho}^2\,\mathrm{d}z + \int_{-H}^{0} \overline{\left(\rho^{\text{inter}}_{\text{BT}}\right)^2}\,\mathrm{d}z + \int_{-H}^{0} \overline{\left(\rho^{\text{inter}}_{\text{BC}}\right)^2}\,\mathrm{d}z + \int_{-H}^{0} \overline{\rho^2_{\text{HF}}}\,\mathrm{d}z. \tag{23}$$

The first term on the rhs is the vertically integrated squared mean density, the second and third terms, the vertically integrated interannual density variance, split between its barotropic and baroclinic parts and the last term the high-frequency density variance which contains all resolved sub annual frequencies. These four reservoirs are schematically shown in Figure 6 as black boxes. The focus here is on all the transfers toward or from the barotropic density variance which is proportional to the steric sea level variance. Indeed, using Equation 21, it is easily seen that:

$$\overline{\left(\eta^{inter}\right)^2} = \frac{H}{\rho_0^2}\int_{-H}^{0} \overline{\left(\rho^{inter}_{BT}\right)^2}\,\mathrm{d}z. \tag{24}$$

Thus, the budget for the vertical integral of $\left(\rho^{inter}_{BT}\right)^2$ is the same as the budget for the steric sea level variance, up to a factor $\frac{H}{\rho_0^2}$. Note that we add "unresolved eddies" to the high-frequency density variance reservoir in Figure 6 to be coherent with the transfer made by the parametrized GM eddy induced velocities, we thus implicitly assume that the parametrized eddies have subannual frequencies.

5.2. Equation for the Evolution of the Barotropic Density Variance

An equation for the evolution of the interannual barotropic density is obtained by vertically integrating the product of Equation 7 and $\frac{1}{H}$:

$$\frac{\partial \rho^{\text{inter}}_{\text{BT}}}{\partial t} = \text{ADV}_{\text{BT}} + \text{DIF}_{\text{BT}} + \text{FLU}_{\text{BT}}, \tag{25}$$

where $X_{\text{BT}} = \frac{1}{H}\int_{-H}^{0} X\,\mathrm{d}z$ with X being ADV, DIF or FLU. Multiplying this equation by $\rho^{\text{inter}}_{\text{BT}}$ and integrating vertically give the evolution equation for the vertically integrated $\rho^{\text{inter}}_{\text{BT}}$ variance:

$$\int_{-H}^{0} \overline{\frac{1}{2}\frac{\partial\left(\rho^{\text{inter}}_{\text{BT}}\right)^2}{\partial t}}\,\mathrm{d}z = H\overline{\rho^{inter}_{\text{BT}}\text{ADV}_{\text{BT}}} + H\overline{\rho^{\text{inter}}_{\text{BT}}\text{DIF}_{\text{BT}}} + H\overline{\rho^{\text{inter}}_{\text{BT}}\text{FLU}_{\text{BT}}}. \tag{26}$$

The first term on the rhs is the effect of advection on the interannual barotropic density variance and is represented by the sum of four blue arrows in Figure 6 (the decomposition of this term will be explained below). The second and third terms respectively represent the effect of interannual barotropic diffusion (green arrow

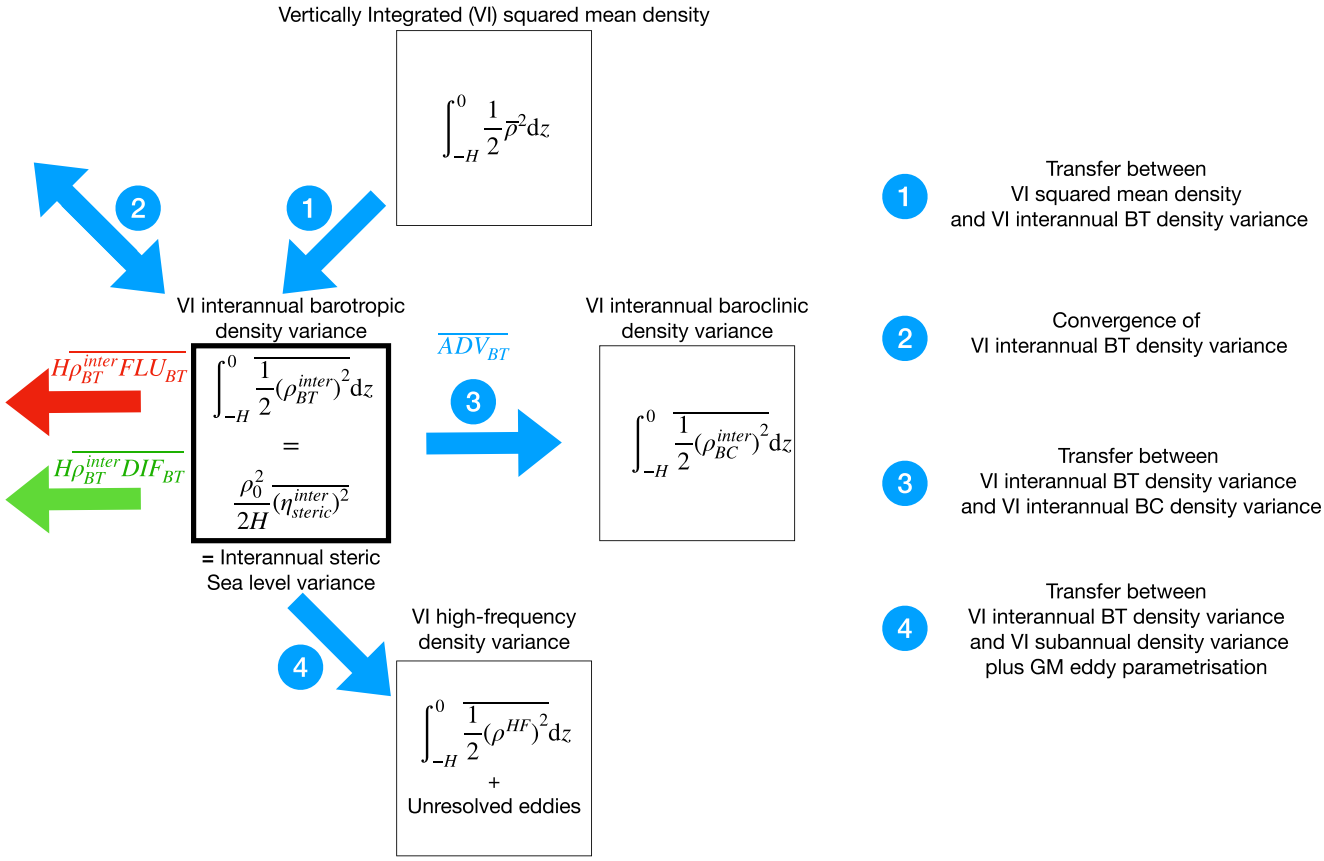

Figure 6. Schematic showing the four reservoirs under consideration here: the Vertically Integrated (VI) squared mean density (top box), the VI interannual barotropic (middle left) and baroclinic (middle right) density variance and the VI high-frequency density variance. The focus is on the interannual barotropic density variance (outlined by a thicker black box) because it is proportional to the interannual steric sea level variance. The red arrow represents the transfer of buoyancy from the atmosphere, the green arrow the diffusion effect and the blue arrows the effect of advection. Advection is decomposed into four terms 1, 2, 3, and 4 explained in the schematic. Note that because we attribute the term due to the GM parameterization of eddy induced velocities to the transfer between interannual and HF density variance, the HF density variance is assumed to also contains the unresolved eddies. The directions of the different arrows are chosen to represent the sign of each transfer when horizontally integrated over the total ocean area (see Table 1). The transfer is a source (sink) when it is directed toward (from) the interannual barotropic density variance reservoir, the only exception is the interannual BT density variance convergence represented by blue arrow 2 which disappears when horizontally integrated.

in Figure 6) and interannual barotropic buoyancy flux from the atmosphere (red arrow in Figure 6). Using the decomposition given by Equation 13 in the advective term gives:

$$H\overline{\rho_{\mathrm{BT}}^{\mathrm{inter}}\mathrm{ADV}_{\mathrm{BT}}} = \overline{\rho_{\mathrm{BT}}^{\mathrm{inter}}\int_{-H}^{0}\mathrm{adv}_1\,\mathrm{d}z} + \overline{\rho_{\mathrm{BT}}^{\mathrm{inter}}\left(\int_{-H}^{0}(\mathrm{adv}_2+\mathrm{adv}_3)\,\mathrm{d}z\right)} + \overline{\rho_{\mathrm{BT}}^{\mathrm{inter}}\int_{-H}^{0}\mathrm{adv}_4\,\mathrm{d}z}. \quad (27)$$

We interpret below the different terms of this decomposition.

5.3. Transfer From the Squared Mean Density

The product of $\int_{-H}^{0}\mathrm{adv}_1\mathrm{d}z$ and $\rho_{\mathrm{BT}}^{\mathrm{inter}}$ can be written as:

$$\overline{\rho_{\mathrm{BT}}^{\mathrm{inter}}\int_{-H}^{0}\mathrm{adv}_1\,\mathrm{d}z} = -\int_{-H}^{0}\overline{\rho_{\mathrm{BT}}^{\mathrm{inter}}\mathbf{v}^{\mathrm{inter}}}\cdot\nabla\overline{\rho}\,\mathrm{d}z. \quad (28)$$

This term is interpreted as the transfer between the squared mean density reservoir and the interannual barotropic density variance reservoir. It is represented by blue arrow number 1 between the vertically integrated squared mean density reservoir and the barotropic interannual density variance reservoirs in Figure 6. This term has been studied by many authors because it has been identified as a possible source of multidecadal North Atlantic

variability (e.g., Arzel et al., 2018; Colin de Verdière & Huck, 1999; Gastineau et al., 2018; Huck et al., 1999). It is positive when the fluctuating transport of anomalous density $\left(\overline{\mathbf{v}^{\text{inter}}\rho_{\text{BT}}^{\text{inter}}}\right)$ is directed downward the mean density gradient $\left(\nabla\overline{\rho}\right)$ that is, when $\overline{\mathbf{v}^{\text{inter}}\rho_{\text{BT}}^{\text{inter}}}\cdot\nabla\overline{\rho}<0$. An intuitive interpretation is that, in this case, the fluctuating part acts to weaken the mean density gradient by transporting positive density anomalies toward low values of mean density and negative values toward high values of mean density.

5.4. Barotropic Density Variance Convergence and Transfer Between Barotropic and Baroclinic Density Variance

Using the vertical decomposition of the velocity and density into the advective term, first without any timescale decomposition gives:

$$-\nabla\cdot(\mathbf{v}\rho)=-\nabla\cdot(\mathbf{v}_{\text{BT}}\rho_{\text{BT}})-\nabla\cdot(\mathbf{v}_{\text{BC}}\rho_{\text{BT}})-\nabla\cdot(\mathbf{v}_{\text{BT}}\rho_{\text{BC}})-\nabla\cdot(\mathbf{v}_{\text{BC}}\rho_{\text{BC}}). \tag{29}$$

The vertical integral of the terms involving only one BC term is zero and we are thus left with the following expression for the barotropic part of the advective term:

$$\frac{1}{H}\int_{-H}^{0}-\nabla\cdot(\mathbf{v}\rho)\,\mathrm{d}z=-\nabla\cdot(\mathbf{v}_{\text{BT}}\rho_{\text{BT}})-\frac{1}{H}\int_{-H}^{0}\nabla\cdot(\mathbf{v}_{\text{BC}}\rho_{\text{BC}})\,\mathrm{d}z. \tag{30}$$

Applying this vertical decomposition (30) to the sum of terms adv_3 and adv_4 from (13) gives (see details in Appendix C):

$$\overline{\rho_{\text{BT}}^{\text{inter}}\int_{-H}^{0}(\text{adv}_3+\text{adv}_4)\,\mathrm{d}z}=-\nabla\cdot\left(\overline{\mathbf{V}_{BT}\frac{\left(\rho_{\text{BT}}^{\text{inter}}\right)^2}{2}}\right)-\frac{1}{H}\int_{-H}^{0}\overline{\rho_{\text{BT}}^{\text{inter}}\nabla\cdot\left(\mathbf{V}_{\text{BC}}\rho_{\text{BC}}^{\text{inter}}\right)}\,\mathrm{d}z \tag{31}$$

where $\mathbf{V}_{\text{BT}}=\overline{\mathbf{v}_{\text{BT}}}+\mathbf{v}_{\text{BT}}^{\text{inter}}$ and $\mathbf{V}_{BC}=\overline{\mathbf{v}_{\text{BC}}}+\mathbf{v}_{\text{BC}}^{\text{inter}}$. In this formula, the first term on the rhs is the convergence of the interannual barotropic density variance by the sum of the mean barotropic and interannual barotropic velocities. This term disappears when integrated horizontally and thus cannot be a global source or sink of interannual barotropic density variance, it is represented by blue arrow number 2 in Figure 6. The last term in the rhs is the transfer between the interannual baroclinic and barotropic density variance, it is represented by blue arrow number 3 in Figure 6. The convergence and transfer terms are plotted in Figure 7, the convergence of interannual barotropic density variance is almost everywhere smaller than the transfer between the barotropic and baroclinic interannual density variance. This is not surprising since the baroclinic part of the circulation is much larger than the barotropic part almost everywhere. This term is qualitatively similar to $\overline{\text{ADV}^2_{\text{steric}}}$ (see Figure 4), the term due to the advection of density anomalies by the time mean velocity, which dominates over $\overline{\text{ADV}^3_{\text{steric}}}$. It is mostly positive in the Indian ocean, indicating that the baroclinic/barotropic transfer is, in this region, a source of interannual steric sea level variance and have both sign in the equatorial Pacific ocean. Its spatial integral is equal to the sum of the spatial integral of terms $\overline{\text{ADV}^2_{\text{steric}}}$ and $\overline{\text{ADV}^3_{\text{steric}}}$ and is thus weakly negative (-0.3×10^{-12} m^2 s^{-1}). Note that in Figure 7, the formula from Equation 31 has been rescaled by $H\rho_0^2$ to correspond to the steric sea level (following Equation 24) which is the focus of this article.

5.5. Transfer to HF Density Variance and GM Parameterization of Eddy Velocity

The last term is:

$$\rho_{\text{BT}}^{\text{inter}}\int_{-H}^{0}\text{adv}_4\,\mathrm{d}z=\rho_{\text{BT}}^{\text{inter}}\int_{-H}^{0}R_{\text{HF}}\,\mathrm{d}z. \tag{32}$$

This term is a sink of barotropic variance (Figure 6). The HF has already been identified in Hochet et al. (2020); Hochet et al. (2022) as acting as a damping effect on the lower frequencies. This induces a density variance transfer from low to high frequencies, consistently with local observations near the Drake passage (Sévellec et al., 2021). High frequencies associated with smaller spatial scales tend to erode the large scale gradients associated with low frequencies. Because of the link between the density variance and the QG APE it can also be thought as a direct APE cascade in the temporal scale as explained in Arbic et al. (2014). As mentioned in last

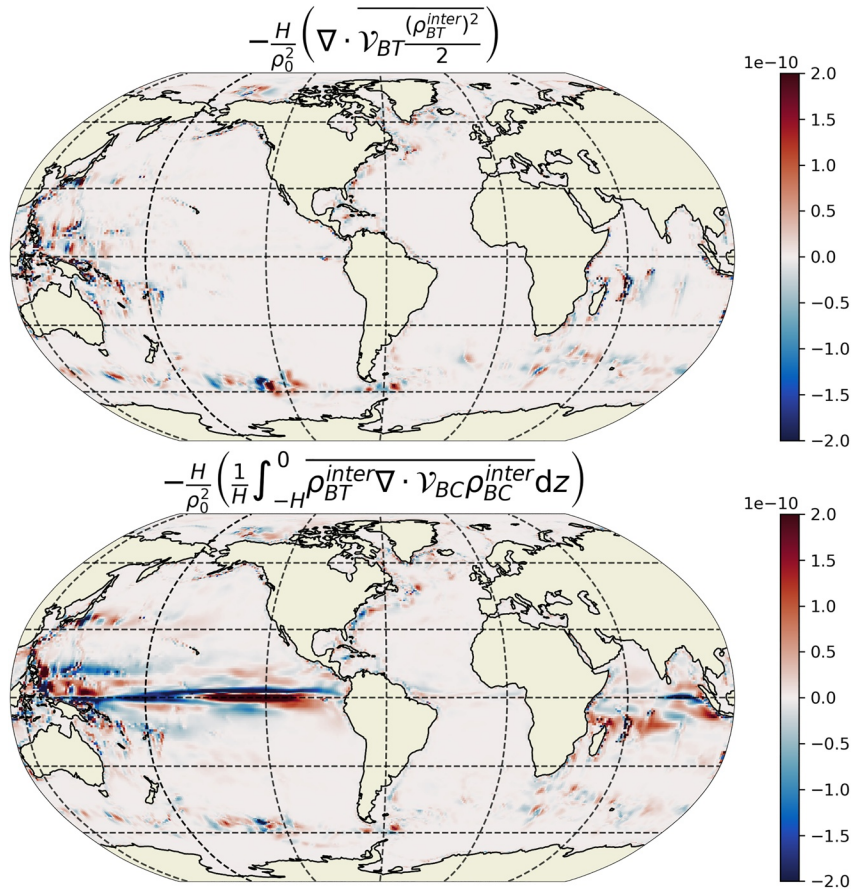

Figure 7. Decomposition of the sum of $\overline{\mathrm{ADV}^2_{\mathrm{steric}}} + \overline{\mathrm{ADV}^3_{\mathrm{steric}}}$ (in $\mathrm{m}^2\ \mathrm{s}^{-1}$) as the sum of the convergence of interannual barotropic density variance due to mean and interannual velocities (top panel) and the transfer between the interannual barotropic and baroclinic density variance (bottom panel). The two corresponding formulas in Equation 31 have been rescaled by $H\rho_0^2$ (following Equation 24) for easier comparison with the steric sea level terms $\overline{\mathrm{ADV}^2_{\mathrm{steric}}}$ and $\overline{\mathrm{ADV}^3_{\mathrm{steric}}}$ from Figure 4.

section, in ECCO V4r3, this transfer is dominated by the term linked with GM eddy induced velocities rather by the resolved subannual circulation. This transfer is represented by the blue arrow 4 in Figure 6.

6. Conclusion and Discussion

In this article we have developed a new diagnostic based on interannual steric sea level variance budget that allows to robustly assess the sources and sinks of interannual steric sea level variability. Using the ECCO V4r3 state estimate, we have shown that in most regions, the main equilibrium is between the advection which is a source of steric sea level variance and the buoyancy flux from the atmosphere which is a sink of variance. The atmospheric buoyancy flux is largely dominated by the net heat flux exchange with the atmosphere. When horizontally integrated, the diffusive term is one order of magnitude smaller than the advection and the atmospheric buoyancy flux. The advective term can further be decomposed into four different terms which can be associated to different barotropic density variance transfers between different density variance reservoirs. The decomposition of the advection reveals that the main source of interannual variability is the self advection of interannual barotropic density anomalies in the direction opposite to the mean density gradient. In this process, the interannual circulation extracts energy from the mean circulation by eroding the large scale mean density gradient. This term is interpreted as a transfer of barotropic density variance between the mean and the interannual density variance. The same term was previously found to be one of the possible source of the Atlantic multidecadal variability (e.g., Arzel et al., 2018, and references therein). It is then shown that the velocities associated with this transfer are mainly the result of interannual variations of the surface wind stress by means of the Ekman balance. This source term is thus an intrinsic transfer of energy between two oceanic reservoirs triggered by an atmospheric source of variability.

This advective source of interannual steric sea level variance is partly compensated by the term linked with the GM parameterization of eddy induced velocities and by the resolved subannual oceanic circulation. Resolved subannual frequencies and parametrized eddies erode the interannual density gradient and thus act as a sink of interannual steric sea level variability. In this work high frequencies contain every subannual time scales including the seasonal cycle. It is somehow more traditional in physical oceanography to sum the seasonal cycle with the mean circulation to create a climatology. However the non-linear transfer of QG-APE is from low to high frequencies and we thus believe that it is more physically-sound to use the ordered frequency separation as done in this work. Preliminary results not shown here further suggest that the energy exchange between the seasonal cycle and interannual time scales is negligible.

Locally in the Equatorial Pacific, the transfer between the vertically integrated interannual barotropic and baroclinic density variance acts as important sink and source of steric sea level variance. However, when horizontally integrated this term is weakly negative and thus a global sink of interannual steric sea level variance. It is also interesting to note that, in the Equatorial Pacific, variations of the surface freshwater fluxes from the atmosphere act as a source of interannual steric sea level variance.

An important limitation of this study is the absence of explicit turbulence in the ECCO V4r3 state estimate due to its laminar resolution and thus to its parametrization through the GM scheme. We have assumed in this article that the parameterized eddies are only made of subannual time scales which might not be true everywhere (i.e., permanent eddies or eddies evolving on interannual time scales). Moreover, satellite data and high-resolution numerical simulations suggest that high levels of steric sea level interannual variability occur in high energetic regions such as in western boundary currents or in the Antarctic Circumpolar Current (see for instance Figure 1 in Carret et al., 2021). Future work should thus include the effect of a turbulent field in order to (a) avoid the use of an eddy parameterization that might introduce bias in the results and (b) understand the mechanisms of steric sea level variance in these eddy-rich regions. Indeed, mesoscale eddies are expected to induce an inverse kinetic energy cascade in both space and time that results in steric sea level variability at interannual time scales (Arbic et al., 2014; Sérazin et al., 2015). However, the kinetic energy is not the most obvious proxy for steric sea level variance compared to the APE, for which the cascade is direct (as suggested by the pioneering work on oceanic turbulence of Rhines (1977); Salmon (1978, 1980)). Hence, the HF rectification term by which the HF circulation act as a sink on interannual steric sea level variability is expected to remain a sink even in the presence of eddy turbulence, consistently with the present study. The role of the indirect cascade of kinetic energy for the steric sea level variance budget remains unclear and will therefore be the subject of future work. Another potential limitation of this study is the use of a reanalysis (ECCO V4r3) that adjusts the set of initial conditions, parameters, and atmospheric boundary conditions to fit observations. The ECCO V4 state estimate, contrary to others reanalysis products, obeys the law of physics, but the fitting procedure might nonetheless induce bias in some of the correlations computed in this article. A perspective would thus be to compare our results with that obtained in a forced or free oceanic run containing eddy turbulence such as DRAKKAR 112° (Molines et al., 2014) simulations for instance.

Finally the steric sea level variance budget appears to be a relatively simple tool to understand the mechanisms controlling the steric sea level variability. It could thus be used to help improve the representation of steric sea level variability in different models, for instance in climate models used for future climate projections, by facilitating the comparison of the representation of the physical mechanisms at play in these models.

Appendix A: HF Rectification Term in the Decomposition of the Advection

The high frequency rectification term adv_4 from Equation 13 is given by:

$$\mathrm{adv}_4 = -\nabla\cdot\left(\mathbf{v}^{\mathrm{inter}}\rho^{\mathrm{HF}}\right) - \nabla\cdot\left(\mathbf{v}^{\mathrm{HF}}\rho^{\mathrm{inter}}\right) - \nabla\cdot\left(\mathbf{v}^{\mathrm{HF}}\rho^{\mathrm{HF}}\right) + R_{\mathrm{GM}}. \tag{A1}$$

where R_{GM} represents the effect of the eddy-induced velocities associated with the GM parameterization (Gent & McWilliams, 1990).

Appendix B: Squared Density Decomposition

The square of Equation 22 is:

$$\begin{aligned}\rho^2 = \overline{\rho}^2 + \left(\rho_{\mathrm{BT}}^{\mathrm{inter}}\right)^2 + \left(\rho_{\mathrm{BC}}^{\mathrm{inter}}\right)^2 + \left(\rho^{\mathrm{HF}}\right)^2 + 2\overline{\rho}\left(\rho_{\mathrm{BT}}^{\mathrm{inter}} + \rho_{\mathrm{BC}}^{\mathrm{inter}} + \rho^{\mathrm{HF}}\right)\\ + 2\left(\rho_{\mathrm{BT}}^{\mathrm{inter}}\rho_{\mathrm{BC}}^{\mathrm{inter}} + \rho_{\mathrm{BT}}^{\mathrm{inter}}\rho_{\mathrm{HF}}^{\mathrm{inter}} + \rho_{\mathrm{BC}}^{\mathrm{inter}}\rho_{\mathrm{HF}}\right).\end{aligned} \tag{B1}$$

Time averaging gives:

$$\overline{\rho^2} = \overline{\rho}^2 + \overline{\left(\rho_{\mathrm{BT}}^{\mathrm{inter}}\right)^2} + \overline{\left(\rho_{\mathrm{BC}}^{\mathrm{inter}}\right)^2} + \overline{(\rho^{HF})^2} + 2\overline{\left(\rho_{\mathrm{BT}}^{\mathrm{inter}}\rho_{\mathrm{BC}}^{\mathrm{inter}}\right)}. \tag{B2}$$

Then computing the vertical integral gives the decomposition of the vertically integrated density variance into 4 components:

$$\int_{-H}^{0} \overline{\rho^2}\,\mathrm{d}z = \int_{-H}^{0} \overline{\rho}^2\,\mathrm{d}z + \underbrace{\int_{-H}^{0} \overline{\left(\rho_{\mathrm{BT}}^{\mathrm{inter}}\right)^2}\,\mathrm{d}z}_{=H\overline{\left(\rho_{\mathrm{BT}}^{\mathrm{inter}}\right)^2}} + \int_{-H}^{0} \overline{\left(\rho_{\mathrm{BC}}^{\mathrm{inter}}\right)^2}\,\mathrm{d}z + \int_{-H}^{0} \overline{(\rho^{\mathrm{HF}})^2}\,\mathrm{d}z. \tag{B3}$$

where the fact that $\int_{-H}^{0} \rho_{BC}^{\mathrm{inter}}\rho_{\mathrm{BT}}^{\mathrm{inter}}\mathrm{d}z = \rho_{\mathrm{BT}}^{\mathrm{inter}}\int_{-H}^{0} \rho_{\mathrm{BC}}^{\mathrm{inter}}\mathrm{d}z = 0$, by definition of $\rho_{\mathrm{BC}}^{\mathrm{inter}}$, and $\int_{-H}^{0} \rho_{\mathrm{BT}}^{\mathrm{inter}}\mathrm{d}z = H\rho_{\mathrm{BT}}^{\mathrm{inter}}$, by definition of $\rho_{\mathrm{BT}}^{\mathrm{inter}}$, have been used.

Appendix C: Decomposition of the Advective Terms Linked with adv_2 and adv_3

Inserting adv_2 in Equation 30 gives:

$$\frac{1}{H}\int_{-H}^{0} -\nabla\cdot\left(\overline{\mathbf{v}}\rho^{\mathrm{inter}}\right)\mathrm{d}z = -\nabla\cdot\left(\overline{\mathbf{v}_{\mathrm{BT}}}\rho_{\mathrm{BT}}^{\mathrm{inter}}\right) - \frac{1}{H}\int_{-H}^{0} \nabla\cdot\left(\overline{\mathbf{v}_{\mathrm{BC}}}\rho_{\mathrm{BC}}^{\mathrm{inter}}\right)\mathrm{d}z \tag{C1}$$

similarly, inserting adv_3 in Equation 30 gives:

$$\frac{1}{H}\int_{-H}^{0} -\nabla\cdot\left(\mathbf{v}^{\mathrm{inter}}\rho^{\mathrm{inter}}\right)\mathrm{d}z = -\nabla\cdot\left(\mathbf{v}_{BT}^{\mathrm{inter}}\rho_{\mathrm{BT}}^{\mathrm{inter}}\right) - \frac{1}{H}\int_{-H}^{0} \nabla\cdot\left(\mathbf{v}_{\mathrm{BC}}^{\mathrm{inter}}\rho_{\mathrm{BC}}^{\mathrm{inter}}\right)\mathrm{d}z \tag{C2}$$

Then, summing these two equations, multiplying by $\rho_{\mathrm{BT}}^{\mathrm{inter}}$ and time averaging, we recover Equation 31.

Data Availability Statement

This study uses the following data: ECCO V4r3 which can be found here: https://ecco-group.org/products.htm.

Acknowledgments
ECCO V4r3 salinity and temperature budget computations were greatly facilitated by the existence of the *ecco_v4_py* Python library, and by several tutorials which can be found at: https://ecco-v4-python-tutorial.readthedocs.io/. We warmly acknowledge the authors of this work. This work was also supported by the French National Programme LEFE (Les Enveloppes Fluides de l'Environnement)—GMMC (Groupe Mission Mercator-Coriolis) by the CRATERE project. We thank two anonymous reviewers for their valuable comments and suggestions.

References

Arbic, B. K., Müller, M., Richman, J. G., Shriver, J. F., Morten, A. J., Scott, R. B., et al. (2014). Geostrophic turbulence in the frequency–wavenumber domain: Eddy-driven low-frequency variability. *Journal of Physical Oceanography*, *44*(8), 2050–2069. https://doi.org/10.1175/jpo-d-13-054.1

Arzel, O., Huck, T., & Colin de Verdière, A. (2006). The different nature of the interdecadal variability of the thermohaline circulation under mixed and flux boundary conditions. *Journal of Physical Oceanography*, *36*(9), 1703–1718. https://doi.org/10.1175/jpo2938.1

Arzel, O., Huck, T., & Colin de Verdière, A. (2018). The internal generation of the Atlantic Ocean interdecadal variability. *Journal of Climate*, *31*(16), 6411–6432. https://doi.org/10.1175/jcli-d-17-0884.1

Buckley, M. W., Ponte, R. M., Forget, G., & Heimbach, P. (2014). Low-frequency SST and upper-ocean heat content variability in the North Atlantic. *Journal of Climate*, *27*(13), 4996–5018. https://doi.org/10.1175/jcli-d-13-00316.1

Carret, A., Llovel, W., Penduff, T., & Molines, J.-M. (2021). Atmospherically forced and chaotic interannual variability of regional sea level and its components over 1993–2015. *Journal of Geophysical Research: Oceans*, *126*(4), e2020JC017123. https://doi.org/10.1029/2020jc017123

Cazenave, A., & Llovel, W. (2010). Contemporary sea level rise. *Annual Review of Marine Science*, *2*(1), 145–173. https://doi.org/10.1146/annurev-marine-120308-081105

Colin de Verdière, A., & Huck, T. (1999). Baroclinic instability: An oceanic wavemaker for interdecadal variability. *Journal of Physical Oceanography*, *29*(5), 893–910. https://doi.org/10.1175/1520-0485(1999)029<0893:biaowf>2.0.co;2

Durand, F., Piecuch, C. G., Becker, M., Papa, F., Raju, S. V., Khan, J. U., & Ponte, R. M. (2019). Impact of continental freshwater runoff on coastal sea level. *Surveys in Geophysics*, *40*(6), 1437–1466. https://doi.org/10.1007/s10712-019-09536-w

Forget, G., Campin, J.-M., Heimbach, P., Hill, C. N., Ponte, R. M., & Wunsch, C. (2015). ECCO version 4: An integrated framework for non-linear inverse modeling and global ocean state estimation [Dataset]. Geoscientific Model Development, *8*(10), 3071–3104. https://doi.org/10.5194/gmd-8-3071-2015

Fukumori, I., Wang, O., & Fenty, I. (2021). Causal mechanisms of sea level and freshwater content change in the Beaufort Sea. *Journal of Physical Oceanography*, *51*(10), 3217–3234. https://doi.org/10.1175/JPO-D-21-0069.1

Gastineau, G., Mignot, J., Arzel, O., & Huck, T. (2018). North Atlantic Ocean internal decadal variability: Role of the mean state and ocean-atmosphere coupling. *Journal of Geophysical Research: Oceans*, *123*(8), 5949–5970. https://doi.org/10.1029/2018jc014074

Gent, P. R., & McWilliams, J. C. (1990). Isopycnal mixing in ocean circulation models. *Journal of Physical Oceanography*, *20*(1), 150–155. https://doi.org/10.1175/1520-0485(1990)020<0150:imiocm>2.0.co;2

Gill, A. E., & Niiler, P. P. (1973). The theory of the seasonal variability in the ocean. *Deep-Sea Research*, *20*(2), 141–177. https://doi.org/10.1016/0011-7471(73)90049-1

Gregory, J., Griffies, S., Hughes, C., Lowe, J. A., Church, J. A., Fukimori, I., et al. (2019). Concepts and terminology for sea level: Mean, variability and change, both local and global. *Surveys in Geophysics*, *40*(6), 1251–1289. https://doi.org/10.1007/s10712-019-09525-z

Hochet, A., Huck, T., Arzel, O., Sévellec, F., & Colin de Verdière, A. (2022). Energy transfers between multidecadal and turbulent variability. *Journal of Climate*, *35*(4), 1157–1178. https://doi.org/10.1175/jcli-d-21-0136.1

Hochet, A., Huck, T., Arzel, O., Sévellec, F., Colin de Verdière, A., Mazloff, M., & Cornuelle, B. (2020). Direct temporal cascade of temperature variance in eddy-permitting simulations of multidecadal variability. *Journal of Climate*, *33*(21), 9409–9425. https://doi.org/10.1175/jcli-d-19-0921.1

Huck, T., Colin de Verdière, A., & Weaver, A. J. (1999). Interdecadal variability of the thermohaline circulation in box-ocean models forced by fixed surface fluxes. *Journal of Physical Oceanography*, *29*(5), 865–892. https://doi.org/10.1175/1520-0485(1999)029<0865:ivottc>2.0.co;2

Jackett, D. R., & Mcdougall, T. J. (1995). Minimal adjustment of hydrographic profiles to achieve static stability. *Journal of Atmospheric and Oceanic Technology*, *12*(2), 381–389. https://doi.org/10.1175/1520-0426(1995)012<0381:maohpt>2.0.co;2

Llovel, W., Fukumori, I., & Meyssignac, B. (2013). Depth-dependent temperature change contributions to global mean thermosteric sea level rise from 1960 to 2010. *Global and Planetary Change*, *101*, 113–118. https://doi.org/10.1016/j.gloplacha.2012.12.011

Llovel, W., Guinehut, S., & Cazenave, A. (2010). Regional and interannual variability in sea level over 2002–2009 based on satellite altimetry, Argo float data and GRACE ocean mass. *Ocean Dynamics*, *60*(5), 1193–1204. https://doi.org/10.1007/s10236-010-0324-0

Llovel, W., & Lee, T. (2015). Importance and origin of halosteric contribution to sea level change in the southeast Indian Ocean during 2005–2013. *Geophysical Research Letters*, *42*(4), 1148–1157. https://doi.org/10.1002/2014GL062611

Lombard, A., Cazenave, A., Le Traon, P.-Y., & Ishii, M. (2005). Contribution of thermal expansion to present-day sea-level change revisited. *Global and Planetary Change*, *47*(1), 1–16. https://doi.org/10.1016/j.gloplacha.2004.11.016

Meyssignac, B., Piecuch, C. G., Merchant, C. J., Racault, M.-F., Palanisamy, H., MacIntosh, C., et al. (2017). Causes of the regional variability in observed sea level, sea surface temperature and ocean colour over the period 1993–2011. *Surveys in Geophysics*, *38*(1), 187–215. https://doi.org/10.1007/s10712-016-9383-1

Molines, J.-M., Barnier, B., Penduff, T., Treguier, A., & Le Sommer, J. (2014). ORCA12.L46 climatological and interannual simulations forced with DFS4.4: GJM02 and MJM88. (Tech. Rep.). *The Drakkar Group: Experiment Report GDRI-DRAKKAR-2014-03-19*, 50. Retrieved from https://www.drakkar-ocean.eu/publications/reports/

Neumann, B., Vafeidis, A. T., Zimmermann, J., & Nicholls, R. J. (2015). Future coastal population growth and exposure to sea-level rise and coastal flooding - A global assessment. *PLoS One*, *10*(3), 1–34. https://doi.org/10.1371/journal.pone.0118571

Nicholls, R. J., & Cazenave, A. (2010). Sea-level rise and its impact on coastal zones. *Science*, *328*(5985), 1517–1520. https://doi.org/10.1126/science.1185782

Piecuch, C., & Ponte, R. (2011). Mechanisms of interannual steric sea level variability. *Geophysical Research Letters*, *38*(15), L15605. https://doi.org/10.1029/2011GL048440

Rhines, P. B. (1977). The dynamics of unsteady currents. *Sea*, *6*, 189–318.

Saji, N., Goswami, B. N., Vinayachandran, P., & Yamagata, T. (1999). A dipole mode in the tropical Indian Ocean. *Nature*, *401*(6751), 360–363. https://doi.org/10.1038/43854

Salmon, R. (1978). Two-layer quasi-geostrophic turbulence in a simple special case. *Geophysical & Astrophysical Fluid Dynamics*, *10*(1), 25–52. https://doi.org/10.1080/03091927808242628

Salmon, R. (1980). Baroclinic instability and geostrophic turbulence. *Geophysical & Astrophysical Fluid Dynamics*, *15*(1), 167–211. https://doi.org/10.1080/03091928008241178

Sérazin, G., Penduff, T., Grégorio, S., Barnier, B., Molines, J.-M., & Terray, L. (2015). Intrinsic variability of sea level from global ocean simulations: Spatiotemporal scales. *Journal of Climate*, *28*(10), 4279–4292. https://doi.org/10.1175/jcli-d-14-00554.1

Sévellec, F., Naveira Garabato, A., & Huck, T. (2021). Damping of climate-scale oceanic variability by mesoscale eddy turbulence. *Journal of Physical Oceanography*, *51*(2), 491–503. https://doi.org/10.1175/jpo-d-20-0141.1

Stammer, D., Cazenave, A., Ponte, R. M., & Tamisiea, M. E. (2013). Causes for contemporary regional sea level changes. *Annual Review of Marine Science*, *5*(1), 21–46. https://doi.org/10.1146/annurev-marine-121211-172406

Vallis, G. K. (2017). *Atmospheric and oceanic fluid dynamics*. Cambridge University Press.

WCRP Global Sea Level Budget Group. (2018). Global sea-level budget 1993–present. *Earth System Science Data*, *10*(3), 1551–1590. https://doi.org/10.5194/essd-10-1551-2018

Willis, J. K., Roemmich, D., & Cornuelle, B. (2004). Interannual variability in upper ocean heat content, temperature, and thermosteric expansion on global scales. *Journal of Geophysical Research*, *109*(C12), C12036. https://doi.org/10.1029/2003JC002260